Alpha dose rate calculations for UO2 based materials using stopping power models

Nuclear Materials and Energy 22 (2020) 100734

Contents lists available at ScienceDirect

Nuclear Materials and Energy

journal homepage: www.elsevier.com/locate/nme

Alpha dose rate calculations for UO_2 based materials using stopping power models

N.L. Hansson[a,*], C. Ekberg[a], K. Spahiu[a,b]

[a] Nuclear Chemistry / Industrial Materials Recycling, Chalmers University of Technology, SE-412 96 Gothenburg, Sweden
[b] Swedish Nuclear Fuel and Waste Management Co., SE-101 24 Stockholm, Sweden

ARTICLE INFO

Keywords:
Dose rate
UO_2
Stopping Power
ASTAR
SRIM
Bethe-Bloch
Lindhard–Scharff

ABSTRACT

Accurate dose rate models for UO_2 based materials in contact with water are important in the modeling of the radiolytically promoted dissolution of spent fuel. Dose rates of α-doped UO_2 and un-irradiated MOX fuel were modelled using the ASTAR and SRIM stopping power databases. Dose rates were calculated as a function of distance from the active surface. Comparisons with common dose rate calculation models and the combined Bethe-Bloch and Lindhard–Scharff (LS) equation were performed. It was shown that the ASTAR and SRIM databases could more accurately simulate an α-spectrum compared to the Bethe-Bloch-LS equation. A comparison between the continuous slowing down approximation (CSDA) and the radial projection algorithm in the SRIM program was performed, and it was shown that CSDA overestimates the range of the α-particles by a few percent. This leads to an overestimation of the α-dose rate at distances close to the maximum range of the α-particle in water. A relationship between the average dose rate to specific α-activity ratio as a function of α-energy was obtained from the calculations, which can easily be implemented in alpha dose rate calculations of a UO_2 based materials.

1. Introduction

In the safety analysis of a geological repository, the oxidative dissolution of the used nuclear fuel in case of a water intrusion scenario determines the source term from the repository. Dissolution of the UO_2-matrix leads to a release of radiotoxic actinides and fission products, the latter which is to a large extent (>90%) contained in the UO_2-matrix [1]. As UO_2 is highly insoluble in the U(IV) state, the dissolution rate is negligible under the reducing groundwater conditions [2]. This is due to reducing minerals present at final repository depths (~500 m) [3]. The main mechanism of fuel dissolution is therefore through the formation of locally oxidizing conditions at the fuel surface through radiolysis of water [4]. The production of radiolytic oxidants depends on the type of radiation and on the dose rate. Low linear energy transfer (LET) radiation, such as beta and gamma radiation produce more radicals, while high LET radiations, such as alpha radiation, results predominantly in the formation of molecular radiolysis products. Alpha radiolysis persists during long repository times and is thus the main contributor to fuel dissolution after a thousand years. Of the radiolytic oxidants, H_2O_2 has a relative impact of >99.9% under an α-radiation field, and other radiolytic oxidants can be neglected [5]. Recent results [6, 7] indicate that a large amount of H_2O_2 decomposes to oxygen and water on the fuel surface, thereby slightly decreasing the importance of H_2O_2 for SIMFUEL in favor of O_2 [8].

To model the radiolytic production of oxidants, the flux and energy distribution of the α-particles leaving the source must be calculated. The crucial parameters in this calculation are the specific α-activity and stopping powers of the attenuating media. The Bethe-Bloch equation, which is at the core of all stopping power models, describes the attenuation of a particle due to electromagnetic interactions in the target material [9, 10]. The stopping power spectrum can be divided into low-, intermediate- and high-speed particle regimes respectively [11]. The Bethe-Bloch equation including shell and density effect corrections, accurately describes ion stopping in the high-speed regime. As the Bethe-Bloch equation has discrepancies compared with experimental data at low and intermediate particle energies (<1 MeV/nucleon, i.e. 4 MeV α-particles) [12], databases using theoretical models that are normalized using experimental data are often utilized [9]. The ASTAR database contains stopping powers between 1 keV and 1 GeV for α-particles in a wide variety of target materials [13]. ASTAR uses the Bethe-Bloch equation in the high energy region, where various correction terms are included. At low energies, stopping powers are based on experimental data which are fitted using numerical coefficients provided by Ziegler [14] and Watt [15]. In the SRIM program, an

* Corresponding author.
E-mail address: nikhans@chalmers.se (N.L. Hansson).

https://doi.org/10.1016/j.nme.2020.100734
Received 6 September 2019; Received in revised form 20 November 2019; Accepted 15 December 2019
Available online 01 February 2020

extensive experimental database is combined with a mathematical model developed by Ziegler [16]. The model includes the Core and Bond (CAB) approach, which accurately describes the effect of binding electrons on the stopping power of compounds, rather than treating the compound as a linear combination of the constituent atoms' stopping powers, i.e. Bragg's Rule [16]. In dose rate and range calculation methods the continuous slowing down approximation (CSDA) is often used which numerically integrates the reciprocal of the stopping power over the considered energy interval [17]. The CSDA approach does not consider any radial projection, i.e. it considers the projectile path to be straight and therefore overestimates the projectile range. The SRIM program is equipped with the Projected Range Algorithm (PRAL) which takes radial projection into account which can be used to estimate the error of the CSDA method.

Despite its limitations, the Bethe-Bloch equation is utilized in dose rate models for nuclear materials [18]. Attempts of extending the Bethe-Bloch equation using experimental data have shown potential when considering the stopping power of low velocity projectiles. One such Bethe-algorithm is obtained from Toftegaard et al. [12], which is based on the original Bethe-equation [10] with density and effective charge corrections at intermediate velocities using the semi-empirical procedure developed by Hubert et al. [19]. In order to extend this equation to a lower energy, it is assumed that the stopping power can be reasonably expressed by the Lindhard–Scharff (LS) equation in the low energy regime [19, 20]. As the first derivative of the combined stopping power equation should be continuous, the LS-equation replaces Bethe-Bloch at energies where this discrepancy is minimized. This combined algorithm is identical to the one used in the SHIELD-HIT code commonly used in particle therapy [12, 21].

In many dose rate models, Monte Carlo methods are utilized to address the stochastic nature of particle emission and attenuation [22, 23]. However, as these are computationally demanding, empirical relationships are often used to calculate dose rates from used nuclear fuel or doped UO_2 as well as ranges of α-particles [24–26]. A commonly used [27-30] empirical relationship was developed by Sunder where the α-particle mass stopping power ratio between H_2O and UO_2 is utilized [31]. Sunder states that the ratio between the mass stopping powers can be approximated by the ratios of the atomic numbers and atomic masses, as in Eq. (1) below:

$$\frac{\left[-\frac{1}{\rho}\frac{dE}{dx}\right]_{H_2O}}{\left[-\frac{1}{\rho}\frac{dE}{dx}\right]_{UO_2}} = \frac{\left[\frac{Z}{A}\right]_{H_2O}}{\left[\frac{Z}{A}\right]_{UO_2}} = 1.39 \tag{1}$$

This is based on the assumption that the Bethe-Bloch equation is a weak function of the ionization energy. This is supported by the author by using experimental linear stopping power data reported by Spinks and Woods and Nitzki and Matzke for water and UO_2 respectively, for a projectile energy 5.3 MeV, as $[-dE/dx]_{H2O} = 43$ keV/μm and $[-dE/dx]_{UO2} = 325$ keV/μm, resulting in the ratio 1.39 [31, 32]. It should be pointed out that the average linear stopping power literature value for 5.3 MeV α-particles in water according to Spinks and Woods is 136 keV/μm [32]. By using this value, the ratio in Eq. (1) results in 4.33 instead of 1.39, resulting in approximately a factor 3 higher dose rate in the surrounding water. The Sunder method might therefore underestimate the dose-rate in the surrounding water.

Another empirical relationship used in dose rate calculations [22] was derived by Garisto [26], which describes the average energy E_{avg} of α-particles escaping from a planar surface, as shown in Eq. (2) below:

$$E_{avg} = \left(\frac{A}{2\delta_{max}}\right)\left(\frac{2E_0^3}{3} + \frac{B \cdot E_0^2}{A}\right) \tag{2}$$

where A and B are constants provided by Nitzki and Matzke [33] and δ_{max} is the maximum α-particle range in the UO_2 based material. This equation is based on the assumption that 25% of the α-particles emitted in the outer layer with thickness δ_{max}, escape from the surface. It also assumes that the energy dependence of the stopping power can be described by the expression $dE/dx = -(AE + B)^{-1}$ over the considered energy range, based on the work of Nitzki and Matzke [33]. The value 25% originates from the work of Hosoe et al. who derived an expression for the energy spectrum $g(E,E_0)$ of α-particles escaping a planar surface [34]. However, in Hosoe's derivation, the solution for the energy spectrum is given as a function of path length and does as such not consider the emission angle. This is correctly identified by Garisto [26], who derives the angle-dependent energy spectrum $g(E,\theta,E_0)$ as shown in Eq. (3):

$$g(E, \theta, E_0) = 2g(E, E_0)\cos(\theta), \quad 0 \le \theta \le \frac{\pi}{2} \tag{3}$$

The same correction must be made for the escape probability in order to account for the angular dependence. According to the mean value theorem for definite integrals, the mean value of cos(θ) is for $0 \le \theta \le \pi/2$ equal to $2/\pi$, giving an escape probability equal to $(1/4)\cdot(4/\pi) = 1/\pi$ rather than 0.25 for the polar angle θ interval $[-\pi/2, \pi/2]$. An expression of the angle-corrected $E_{avg,\theta}$ can then be derived by using this correction factor together with Eq. (2), yielding the angle-corrected expression of $E_{avg,\theta}$ as shown in Eq. (4):

$$E_{avg,\theta} = \left(\frac{2A}{\pi\delta_{max}}\right)\left(\frac{2E_0^3}{3} + \frac{B \cdot E_0^2}{A}\right) \tag{4}$$

In this modeling study, a geometrical model has been developed in MATLAB 2016b which calculates dose rates in water surrounding different α-doped UO_2 material using the ASTAR and SRIM databases as well as the combined Bethe-Bloch-LS algorithm. From the dose rate calculations, radiolytic H_2O_2-production is calculated as a function of the distance perpendicular to the UO_2-surface. A few different materials with various alpha emitter content are studied, ranging from 2 wt% ^{235}U-enriched UO_2 to a 24 wt% Pu-doped MOX pellet with specific α-activity 4.96 GBq/g. An investigation of the validity of the aforementioned empirical relationships has also been carried out.

2. Methods

2.1. Model description

ASTAR mass stopping power data as well as the combined Bethe-Bloch-LS equation are available in the libdEdx database [12]. The ASTAR mass stopping power tables can also be obtained from the ICRU 49 report. SRIM mass stopping power tables are obtained from the SRIM-2013 program. The dose rate computational model is written in MATLAB 2016b, using the built-in pseudo-random number generator Mersenne Twister, which has good statistical properties [35]. In the model, $n = 10^5$ particles are generated, each at a random depth δ from the interval $[0, \delta_{max}]$, where δ_{max} is the maximum range of an α-particle in the material, and with a random polar angle θ from the interval $[0, \pi/2]$, where 0 is perpendicular to the surface. This polar angle interval corresponds to particles emitted towards the surface. The considered geometry can be seen in Fig. 1. As the considered UO_2-matrix dimensions are vastly larger than the α-particle range in UO_2, any curvature of the pellet can be ignored, and the geometry can be considered planar. The spherical coordinate system can be simplified through acknowledging that the range required to escape the UO_2-surface is independent of the azimuthal angle φ. That means rotating the trajectory by any angle φ, the resulting trajectory will be symmetrical with that for $\varphi = 0$. The θ interval $[\pi/2, \pi]$ would indicate a particle emitted inwards and will therefore not escape the matrix, which is taken into account when calculating the number of escaping particles as θ is isotropically distributed.

2.2. Fuel models

A 2 wt% ^{235}U-enriched UO_2-pellet was modelled as well as

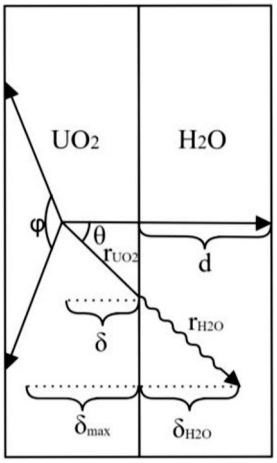

Fig. 1. The planar coordinate system used to illustrate the model geometry.

measured on an α-spectrometer. The considered MOX pellet is 24 wt% Pu-doped with 4.96 GBq/g specific α-activity, 5.44 MeV average emission α-particle energy, 93% theoretical density and a half-cylinder geometry with geometrical surface area of 160.13 mm^2. A more detailed description of the MOX pellet can be found in [27]. The density of the Pu-doped fuel is calculated through a linear interpolation between the densities of UO_2 and PuO_2 [36]. A fuel model with specific activity $5.6{\cdot}10^8$ Bq/g and with α-particle energy of 5.8 MeV as investigated by Cachoir et al. in the EU-Project SFS [18] was also investigated in the present work.

2.3. α-spectrometry

An Ortec, Alpha Duo, Octête α-spectrometer was used for benchmarking the model. A measurement was performed with the 2 wt% ^{235}U-enriched UO_2 with $2.64{\cdot}10^4$ Bq/g specific α-activity, placing the pellet at a couple cm distance from the detector window to ensure a small solid angle.

3. Theory and calculations

The $n = 10^5$ α-particles are attenuated along their path lengths in a stepwise manner using a step-size $s = 0.01$ μm. The path length r_{UO2} required to traverse the UO_2-matrix is calculated from Eq. (5) below:

$$r_{UO_2} = \delta/\cos(\theta) \tag{5}$$

As the α-particles move through the attenuating media, they lose energy and new mass stopping power values are interpolated from the databases. This calculation proceeds for each individual particle until it has stopped or has escaped from the fuel surface.

As the number of modelled particles n is high, an accurate escape probability P_{escape} is obtained from Eq. (6) below:

$$P_{escape} = \frac{n_{E_\alpha \neq 0, r_{UO_2}}}{2n} \tag{6}$$

where $n_{E\alpha\neq0,rUO2}$ is the number of α-particles having non-zero energy after traversing their individual path lengths r_{UO2}. The factor 2 in the denominator takes into account the 50% of particles emitted inwards, as the generated particles are emitted towards the surface in the θ interval [0, π/2]. Using P_{escape}, the total α-particle flux ϕ, (in units Bq), that is escaping the UO_2-surface into the surrounding water layer can be calculated from Eq. (7) below:

$$\phi = P_{escape}{\cdot}\delta_{max}{\cdot}A_{surface}{\cdot}\rho_{UO_2}{\cdot}S_\alpha \tag{7}$$

where $A_{surface}$ is the surface area of the UO_2 based material, ρ_{UO2} is the density of the material and S_α is the specific α-activity (Bq/g). From ϕ, the time period corresponding to the escaping number of particles can be obtained. The benefit of modeling a fixed number of particles instead of a set time period, which would be equivalent for a given particle flux, is that individual particles can easily be studied.

When outside of the UO_2-matrix, mass stopping powers for α-particles in water are interpolated from the databases. In order to calculate the dose rate perpendicular to the UO_2-surface, the distance travelled by the α-particle perpendicular to the surface is calculated. As the α-particles slow down in water, the absorbed energy (in units eV) is stored in the water layers perpendicular to the surface. The dose rate profile $\dot{D}$ (Gy/h) is then calculated from the absorbed energy E_{abs} as a function of perpendicular distance d, through Eq. (8) below:

$$\dot{D}(d) = \frac{\sum_1^{n_{E_\alpha\neq0,rUO_2}} E_{abs}(d){\cdot}1.602{\cdot}10^{-19}{\cdot}3600}{s{\cdot}A_{surface}{\cdot}\rho_{H_2O}} \tag{8}$$

where $1.602{\cdot}10^{-19}$ is the conversion factor from eV to J. As the UO_2 surface area is factored in when calculating ϕ from Eq. (7), the resulting dose rate $\dot{D}$ is surface area independent. In order to calculate the radiolytic H_2O_2 production r_{H2O2}, in units mol/L•s, the dose rate $\dot{D}$ is converted using Eq. (9) below:

$$r_{H_2O_2} = \frac{\dot{D}{\cdot}G_{H_2O_2}{\cdot}\rho_{H_2O}}{1.602{\cdot}10^{-19}{\cdot}N_A{\cdot}3600} \tag{9}$$

where G_{H2O2} is the radiolytic yield, which for α-particles in water is equal to 0.985 molecules/100 eV [37] and N_A is Avogadro's number.

To illustrate the depth and emission angle dependence on the energy of the escaping α-particles, linearly spaced angular and depth vectors with 10^3 steps respectively are used to plot an escape energy surface. See example of this calculation for 24 wt% Pu-doped MOX in Fig. 6.

4. Results

4.1. Mass stopping powers

Mass stopping powers in H_2O and UO_2 from the ASTAR and SRIM databases as well as from the combined Bethe-Bloch-LS equation are shown in Fig. 2. The values between the ASTAR and SRIM stopping power tables agree well with each other but are significantly different from the result obtained using the combined Bethe-Bloch-LS equation for α-particles in UO_2 at low energies. All water stopping power curves show a Bragg-peak characteristic of charged particles. Both ASTAR and SRIM show a Bragg-peak in UO_2, but the Bethe-Bloch-LS equation does not show this tendency.

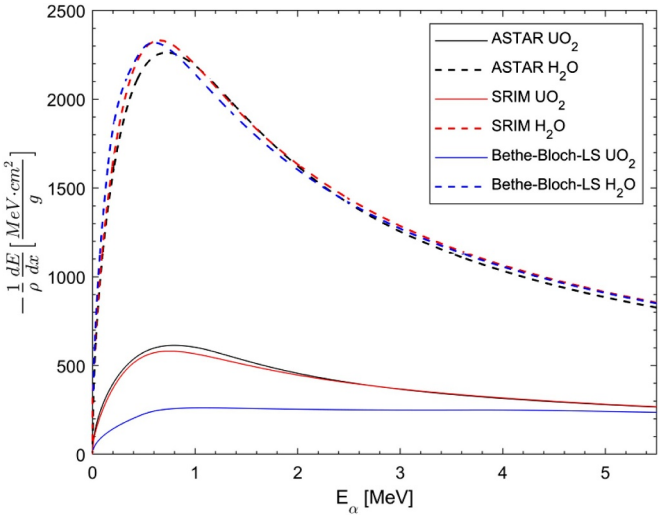

Fig. 2. Mass stopping powers from the Bethe-Bloch-LS equation, ASTAR and SRIM databases for UO_2 and H_2O.

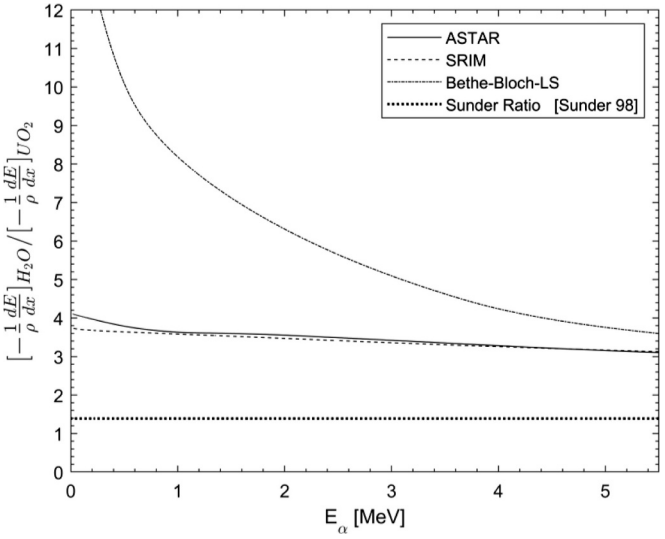

Fig. 3. Ratios between the α-particle stopping powers in H_2O and UO_2 using the ASTAR and SRIM stopping power data as well as the combined Bethe-Bloch-LS equation. A comparison with Sunder's ratio as calculated through Eq. (1). is also shown.

The ratios between the mass stopping powers in water and UO_2 were calculated using the databases and the combined Bethe-Bloch-LS equation, shown in Fig. 3. The ratios are above 3 at all energies in the considered interval and increase with decreasing α-particle energy. The combined Bethe-Bloch-LS equation shows a fairly large deviation from the ASTAR and SRIM ratios, which are themselves fairly consistent with each other. The Sunder ratio from Eq. (1) is also shown for comparison.

Due to the lack of stopping power data for 24 wt% Pu doped MOX, $(U_xPu_{1-x})O_2$ was approximated having the same mass stopping power as UO_2. The validity of this assumption was investigated based on the work of Nitzki and Matzke, where attenuation of α-particles in UO_2 and $(U_{0.8}Pu_{0.2})O_2$ was studied [33]. The approximate relationships provided in [33] have a deviation of less than 1% from their experimental results in the α-particle energy interval 2–8 MeV. A comparison between the stopping powers in UO_2 and $(U_{0.8}Pu_{0.2})O_2$ by using the same approximate relationships is shown in Fig. 4.

The experiments by Nitzi and Matzke are limited to an energy interval of 2–8 MeV but serve as an indication of the validity of the approximation. Using UO_2 as an approximation for $(U_xPu_{1-x})O_2$ is thus

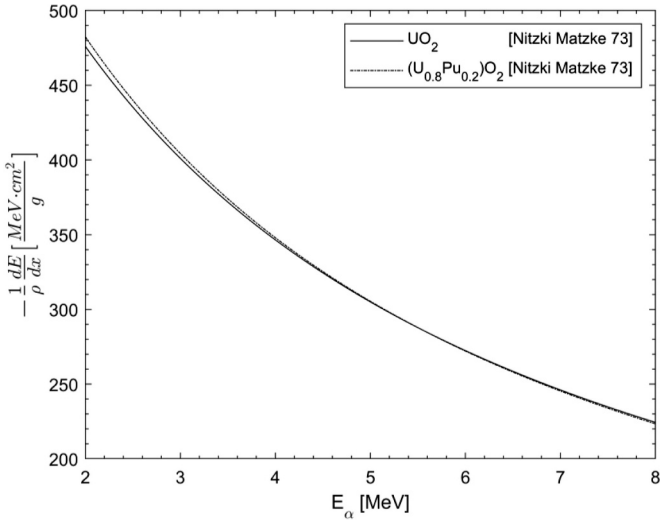

Fig. 4. Comparison of α-particle stopping powers in UO_2 and $(U_{0.8}Pu_{0.2})O_2$ using the approximate relationships established by Nitzki and Matzke.

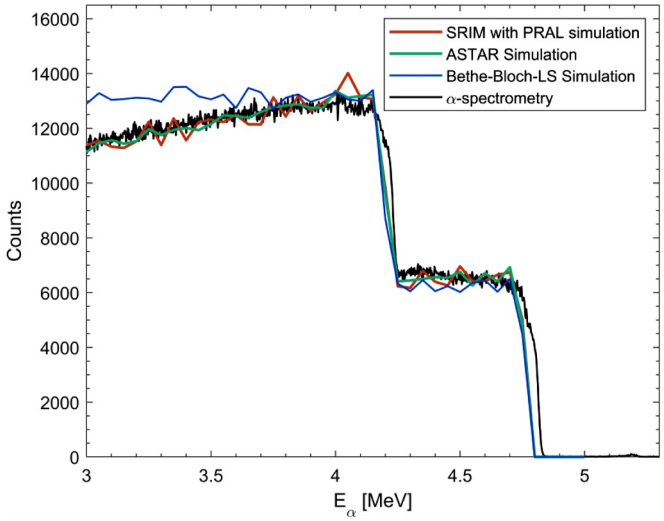

Fig. 5. Simulated and measured UO_2 α-spectrum.

accurate with only a few percent error in the lower end of the energy spectrum studied by Nitzki and Matzke, as seen in Fig. 4.

4.2. Energy spectrum

The α-spectrum of 2 wt% ^{235}U-enriched UO_2 was simulated using ASTAR and SRIM mass stopping power databases and the Bethe-Bloch-LS equation. The simulations were normalized to the measured spectrum. The shape of the simulated spectra shows a clear correspondence with the measured spectrum using a channel width 50 keV in the simulations as compared to 2.44 keV in the detector. The broad channel width is used to smoothen out the simulation, as smaller energy bins requires a very large number of simulated particles to create a smooth distribution between bins. The comparison between the simulated and measured α-spectra are shown in Fig. 5. No significant difference was noted using the SRIM with PRAL data compared with the ASTAR data. Both ASTAR and SRIM data could reproduce the spectrum well using the computational model. However, a minor inconsistency between the SRIM with PRAL simulation and measurement can be observed around 4 MeV. Using the Bethe-Bloch-LS equation, the simulated spectrum overlaps well at energies above 4 MeV. However, below 4 MeV there is a discrepancy with the measured α-spectrum that increases with decreasing α-particle energy.

The simulation of the α-escape energy as a function of emission depth δ and emission angle θ in the 24 wt% Pu MOX-pellet was performed using the ASTAR stopping power data. The resulting escape-energy surface is shown in Fig. 6. The SRIM data is expected to give similar results, as indicated by the UO_2 stopping power data shown in Fig. 2. As the surface shown is for the polar emission angle interval [0, π/2], the fraction of the particles leaving the surface is 0.63. Based on 10^5 generated particles and taking into account the inwards emission angle [π/2, π] as well, 31.5% (P_{escape}) of the particles emitted in the interval [0, δ_{max}] are released from the pellet with an average energy of 3.03 MeV, corresponding to 55.6% of the initial energy $E_0 = 5.44$ MeV, which is illustrated in Fig. 6. The escape probability (31.5%) is therefore very close to the theoretical value of 1/π (31.8%).

The average escape energy $E_{avg,\theta}$ can also be estimated using Eq. (4):

$$E_{avg,\theta} = \left(\frac{2A}{\pi\delta_{max}}\right)\cdot\left(\frac{2E_0^3}{3} + \frac{B\cdot E_0^2}{A}\right) = 3.29\ MeV \tag{10}$$

where $A = 0.362$ μm•MeV^{-2} and $B = 1.15$ μm•MeV^{-1} [33] for the 24 wt% Pu-doped MOX pellet with $E_0 = 5.44$ MeV and $\delta_{max} = 14.11$ μm. $E_{avg,\theta}$ calculated with Eq. (4) gives a 9% higher value than the modelled value of 3.03 MeV. Using the expression derived by Garisto shown in

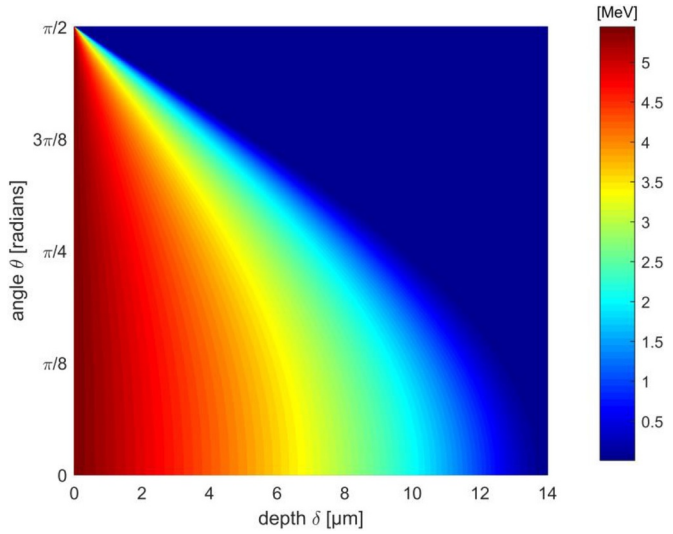

Fig. 6. Release α-particle energy from the 24 wt% Pu MOX surface as a function of emission depth δ and angle θ. The fraction of escaping α-particles is equal to 0.63.

Eq. (2) gives a slightly worse approximation, of 2.59 MeV, 15% lower than the modelled value.

4.3. Dose rate calculation

The ranges of the α-particles in water were calculated using the ASTAR and SRIM with PRAL data and are shown in Fig. 7. The SRIM data were corrected using PRAL to evaluate the significance of radial projection. The data could be fitted to second order polynomials with good accuracy. Below 0.5 MeV the polynomial fits diverge from the calculated ranges, and the intercepts for both the ASTAR and SRIM with PRAL polynomial fits are non-zero. The SRIM with PRAL α-particle range in water is somewhat shorter than the calculated range using the ASTAR data. The empirical relationship for α-particle ranges derived by Jansson and Jonsson is also shown in Fig. 7 [25].

The α-particles that escape the UO_2-matrix produce radiolysis-products in the surrounding water in proportion to their energy loss. The dose rate and H_2O_2 concentration production rate as a function of water depth perpendicular to the MOX-surface was calculated using ASTAR and SRIM with PRAL data combined with G-values [37]. In the 24 wt% Pu-doped MOX with 93% theoretical density, the 5.44 MeV α-particles have a projected range of 13.5 μm using SRIM with PRAL, compared to the 14.1 μm range using the continuous slowing down approximation (CSDA). The SRIM with PRAL and ASTAR dose rate calculation for the MOX pellet are shown in Fig. 8. For the ASTAR data, the average dose rate over the α-particle range in water, corresponding to 43.5 μm water depth is equal to 8.699 kGy/h. The ratio between the average dose rate and the specific α-activity, (Gy/h)/(MBq/g), is equal to 1.754. The SRIM data with PRAL yields an α-particle range equal to 41.7 μm, corresponding to an average dose rate of 8.853 kGy/h and (Gy/h)/(MBq/g) equal to 1.785. As can be seen in Fig. 8, the Bragg-peaks are averaged out when particles are spread out over the emission depths and ranges.

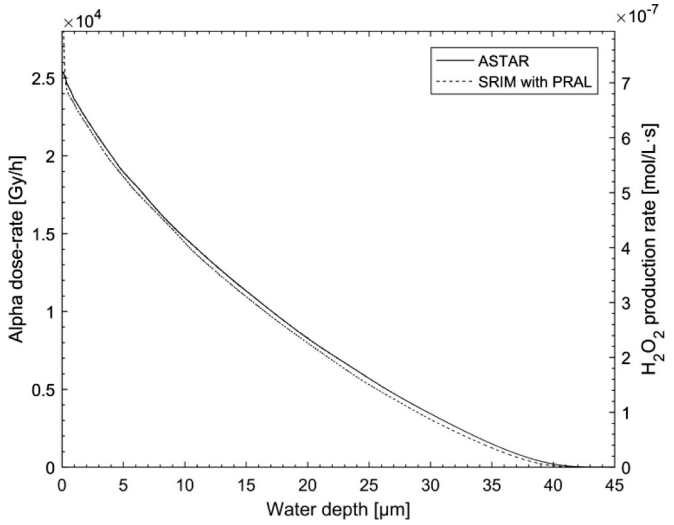

Fig. 8. Dose rate and production rate of H_2O_2 from a 24 wt% doped MOX-pellet as a function of water depth using ASTAR and PRAL corrected SRIM models.

The dose rate model was compared with the Sunder method, using the mass stopping power ratios from Eq. (1) of 1.39 and 4.33. The average escape energy of 3.03 MeV from the ASTAR model was used to find the stopping power at the interface. The comparison can be seen in Fig. 9. The average dose rate using the Sunder method with a mass stopping ratio of 1.39 in the 100 μm water layer is equal to 3.44 kGy/h, which corresponds to (Gy/h)/(MBq/g) = 0.694. For the mass stopping

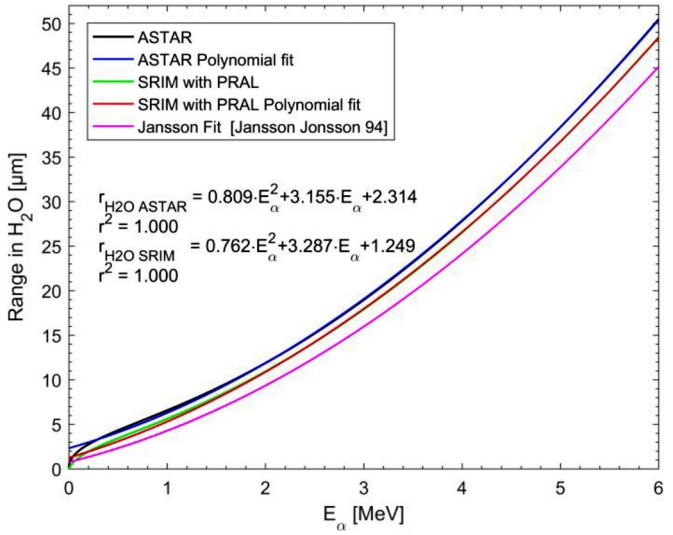

Fig. 7. α-particle ranges in H2O as a function of energy using the ASTAR and SRIM databases as well as the empirical fit by Jansson and Jonsson.

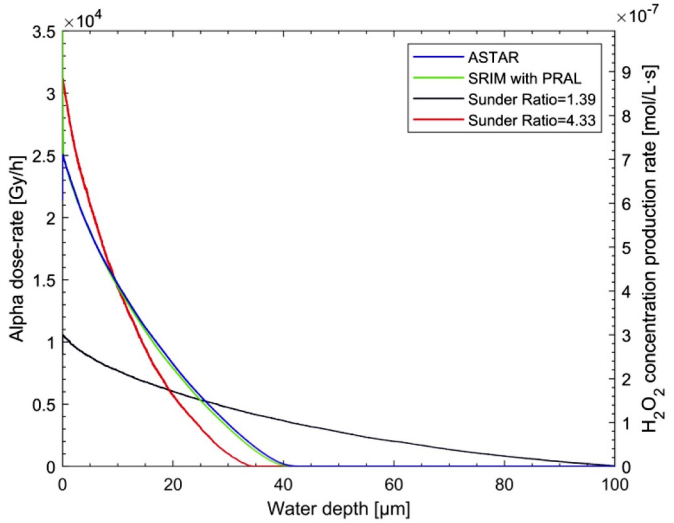

Fig. 9. Comparison of the ASTAR and PRAL corrected SRIM models with the Sunder method.

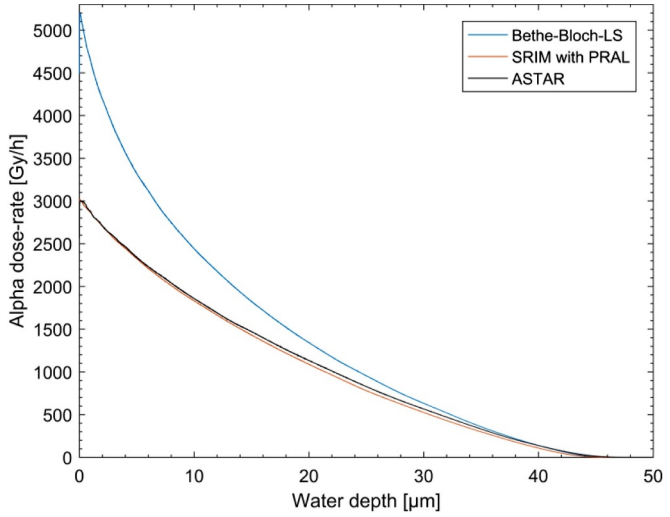

Fig. 10. Dose rate profile using ASTAR and SRIM with PRAL data as well as the Bethe-Bloch-LS equation for the fuel model considered by Cachoir et al. with $E_\alpha = 5.8$ MeV and $5.6 \cdot 10^8$ Bq/g α-activity.

power ratio of 4.33, the average dose rate in the 34.4 μm water layer is equal to 10.05 kGy/h, yielding (Gy/h)/(MBq/g) = 2.027.

The dose rate model was also compared with the Bethe-Bloch model used by Cachoir et al. by adopting their fuel model [18]. The Bethe-Bloch-LS equation shown in Fig. 10 corresponds very well with the results obtained by Cachoir et al. The ASTAR and SRIM with PRAL models gave dose rates that correspond well with each other, as can be seen in Fig. 10. Both gave a significantly lower dose rate as compared with the Bethe-Bloch equation results, especially at low water depths. For the 5.8 MeV α-particles considered in the model of Cachoir et al., the range in water is 47.8 μm using ASTAR data. The dose rate in this water layer equals 1.058 kGy/h, corresponding to (Gy/h)/(MBq/g) = 1.889. The corresponding value using the Bethe-Bloch-LS equation is 46.3 μm, yielding a dose rate of 1.598 kGy/h corresponding to a specific activity ratio (Gy/h)/(MBq/g) = 2.854. Notably, for 5.8 MeV α-particles the Bethe-Bloch-LS equation gave a range in UO_2 equal to 24.0 μm, significantly higher than reported literature values.

The average dose rate to specific α-activity ratios are dependent on the emission α-particle energy of the simulated fuels, as seen from the models of the 24 wt% Pu-doped MOX with 5.44 MeV average α-particle energy (Fig. 8), and the model adopted from Cachoir et al.'s work with 5.8 MeV α-particle energy (Fig. 10) giving different ratios, (Gy/h)/(MBq/g) = 1.754 and 1.889 respectively.

Using a 95% theoretical density UO_2 model with α-particle energy 4.9, 5.2, 5.5 and 5.8 MeV with the ASTAR and SRIM with PRAL databases, the α-energy dependence on the average dose rate to specific α-activity ratio (Gy/h)/(MBq/g) could be calculated. This dependence could accurately be described by linear relationships, as shown in Fig. 11. In order to calculate the total deposited energy in the water-layer surrounding a given α-doped UO_2 material using the relationships, the average α-particle energy as well as the specific α-activity of the material is input together with the α-particle ranges in water as shown on the right y-axis in Fig. 11 (or from the equations in Fig. 7), multiplied by the surface-area. The SRIM with PRAL data gives a somewhat higher average dose rate over the interval, as the α-particle range is shorter which makes the dose concentrated over a shorter range. As seen from Figs. 8 and 9, the dose rate at any given distance is lower. The total deposited energy using the ASTAR data is therefore higher than what is obtained from the SRIM with PRAL simulation.

Using the ASTAR relationship from Fig. 11a. to calculate the 24 wt% Pu-doped MOX pellet, the average dose rate over the α-particle range in water becomes equal to (0.346•5.44–0.120)•4.96 = 8.748 kGy/h, which is very close to the modelled dose rate (Fig. 8) of 8.699 kGy/h. A small variation is expected from the different densities of the 24 wt% Pu-doped MOX and the Cachoir SFS project fuel model, which accounts for the difference.

The dose rate relationships derived in this work can be compared to the spent fuels modelled by Nielsen and Jonsson [24] as well as by Poulesquen et al. [38]. Burnups ranging from 33–55 GWd/t were modelled by the researchers, and the relationship between burnup and specific α-activity from the work of Poulesquen was used to convert the Nielsen data into specific α-activity. The resulting comparison can be seen in Fig. 12. As the average fuel E_α is not stated for the spent fuel models, both 5.2 and 5.5 MeV were used with the ASTAR model from this work.

5. Discussion

Based on the region of validity of the Bethe-Bloch equation, the equation seems unsuitable for describing the attenuation of α-particles in the α-energy spectrum relevant for nuclear fuel. Nitzki and Matzke have compared experimental values for stopping power of α-particles in UO_2 and $(U_xPu_{1-x})O_2$ with the Bethe-Bloch equation [33]. The comparison shows quite an accurate description above 4 MeV, with a growing discprepancy towards the lower energy region. As the α-energy goes below 4 MeV, the disparity becomes large, confirming the region of validity of the Bethe-Bloch equation. This is supported by the α-spectrometry simulation, where the α-energy dependence on the number of counts was poorly described by the Bethe-Bloch-LS equation below 4 MeV. Extending Bethe-Bloch to a lower energy region using the LS-equation does not notably change dose rate calculations compared with the pure Bethe-Bloch equation. This can be concluded by comparing the Bethe-Bloch-LS equation results as seen in Fig. 10 by the results obtained by Cachoir et al. [18], yielding a very similar dose rate curve for the same UO_2-model.

The empirical relationships from Nitzki and Matzke are only accurate in the interval 2–8 MeV, and the mass stopping powers of UO_2 and $(U_xPu_{1-x})O_2$ might deviate below 2 MeV, adding uncertainty to the MOX dose rate calculation in this work. The approximation of E_{avg} derived by Garisto [26] shown in Eq. (2) is based on these same empirical relationships, assuming the stopping power can be described by the expression $dE/dx = -(AE + B)^{-1}$. As seen from Fig. 2, this expression cannot accurately describe the stopping power curve below 1 MeV. After making the angular correction of E_{avg} as seen in Eq. (4), the value of $E_{avg,\theta}$ is still off by 9% compared to the modelled value of the 24 wt% Pu-doped MOX. This indicates that constructing empirical relationships describing properties of the entire energy range based on approximate stopping power relationships in the energy range 2–8 MeV (i.e. $dE/dx = -(AE + B)^{-1}$) is unsuitable.

As secondary electrons are produced when α-particles attenuate, the dose rates in this work are slightly too low as it was assumed these electrons would have a negligible contribution to the dose rate. Electron yields due to the attenuation of α-particles in a U-233 doped pellet has been modelled by Lundgren [39]. It was found that the electron dose rate corresponded to 0.4% of the total dose rate, which serves as an indication of the error due to this assumption.

The ratio of the stopping powers in water and UO_2 obtained from the ASTAR and SRIM stopping power data differs significantly from the suggested ratio in Sunder's work [31], as shown in Fig. 3. These ratios were between 3–5 for α-particles in the investigated energy interval. The combined Bethe-Bloch-LS equation gave a considerably higher stopping power ratio compared to the ASTAR and SRIM data. The stopping power ratios were shown to be somewhat energy dependent, meaning that a constant ratio for the two attenuating media might be inappropriate. The Sunder-calculation method was used in a previous work by our group with the 24 wt% Pu-doped MOX-pellet, yielding an average dose rate of 22.7 kGy/h in the α-particle range in water [27]. The maximum dose rate at the interface was calculated as 85 kGy/h. Both the average and maximum dose rates are approximately a factor 3

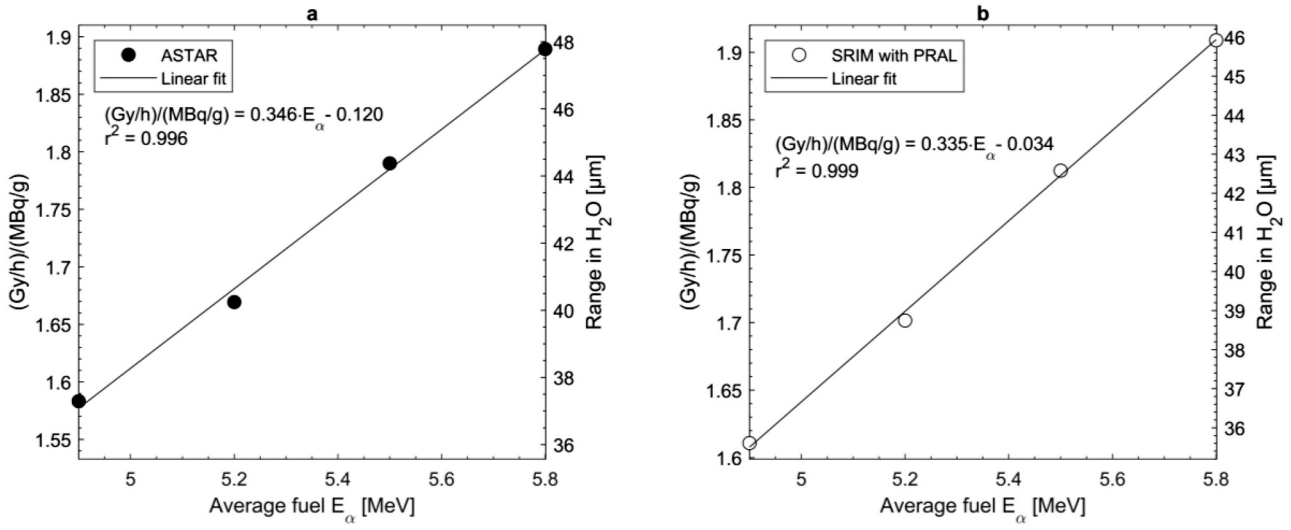

Fig. 11. Average dose rate to specific activity ratio plotted versus the α-particle energy of the fuel, E_α, using the CSDA approach with the ASTAR database (a), as well as the SRIM database with PRAL (b). The average dose rates are calculated for the α-particle ranges in water that are shown on the right y-axes.

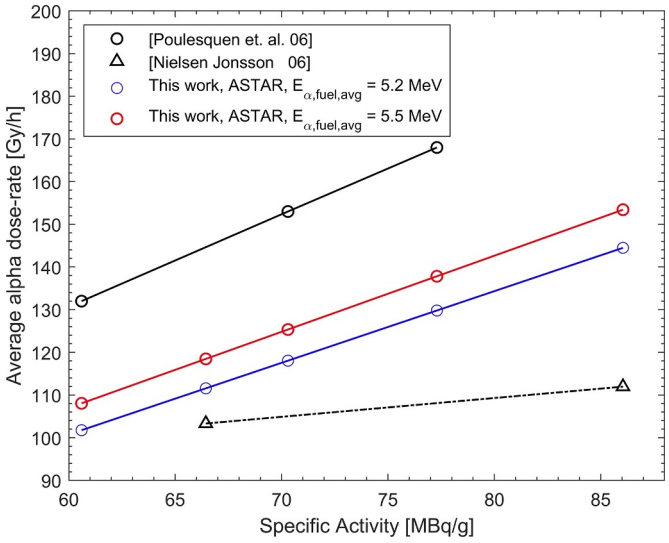

Fig. 12. Comparisons between the ASTAR dose rate model calculated in this work and the dose rate models developed by Poulesquen et al. and Nielsen and Jonsson.

higher than the values obtained in this work. Using Spinks and Woods average literature value yields a stopping power ratio equal to 4.33 instead of 1.39, which corresponds much better with the results obtained in this work, as seen in Fig. 9. The mass stopping power ratio 4.33 resulted in an average dose rate very similar to the ASTAR model from this work, but the dose rate was distributed on a significantly shorter water depth.

The shapes of the calculated dose rate curves in this work are significantly different compared with the one modelled by Poulesquen et al. [38], where there is a factor of approximately 8 between the dose rate at the surface compared with the average dose rate. The calculated ratio between the dose rate at the surface compared with the average dose rate using the computational model in this work yields approximately 3, with a more evenly spread attenuation over the α-particle range. Poulesquen et al.'s simulated particles quickly lose their energy close to the surface and therefore show a different behavior of the dose rate as a function of distance. This might be due to an error in their angular-probability weight-function that gives a high weight to low energy α-particles resulting in a non-isotropic emission, as previously discussed by Tribet et al. [22]. Cachoir et al. use a model similar to the one in this work with an iterative Bethe-Bloch solution, considering all emission depths and angles. The dose rate curve corresponds well with the Bethe-Bloch-LS equation used in this work. The shape of their curve is very similar to the ones obtained using the calculation model derived in this work and the ratio between the maximum and average dose rate is close to 3, showing a consistency between the models.

Linear relationships between dose rate and specific α-activity as a function of α-particle energy was calculated, fitting the simulated data very well. The average dose rate to specific α-activity ratios obtained in this work for 5.2–5.5 MeV α-particles differs somewhat compared to the ratio 2.18 given by Poulesquen et al. [38], approximately 30% higher than the ratios obtained in this work.

6. Conclusion

Stopping power databases using combined experimental and theoretical models such as ASTAR and SRIM are useful for describing the attenuation of α-particles in the energy region that is relevant for nuclear fuels.

The Bethe-Bloch equation with or without the LS-equation extension is not suitable in this energy region and yields too high α-dose rates as compared to the ASTAR and SRIM models. The α-spectrometry results show a good correspondence with the ASTAR and SRIM data, both using the CSDA and PRAL approaches. Using PRAL to estimate the radial projection in the SRIM code indicates that the CSDA approach overestimates the α-particle range by a few percent, while otherwise giving very similar average dose rates. The results in this work suggest a significant improvement to the commonly used empirical relationships regarding dose rate, average escape particle energy as well as α-particle range. This will improve the modeling of radiolytically promoted dissolution of spent fuel. The provided empirical linear relationships between average dose rates and specific α-activity as a function of α-particle emission energy fits the modelled data very well and can straightforwardly be implemented in dose rate calculations of UO_2-materials.

Declaration of Competing Interest

The authors declare that they have no known competing financial interests or personal relationships that could have appeared to influence the work reported in this paper.

Acknowledgements

The Swedish Nuclear Fuel and Waste Management Company, SKB, is gratefully acknowledged for funding of this project. Marcus Hedberg and Thea Lyseid Authen are much appreciated for valuable input.

References

[1] D. Shoesmith, Fuel corrosion processes under waste disposal conditions, J. Nuclear Mater. 282 (1) (2000) 1–31.
[2] D. Rai, M. Yui, D.A. Moore, Solubility and solubility product at 22 C of UO 2 (c) precipitated from aqueous U (IV) solutions, J. Solution Chem. 32 (1) (2003) 1–17.
[3] I. Neretnieks, Some uses for natural analogues in assessing the function of a HLW repository, Chem. Geol. 55 (3–4) (1986) 175–188.
[4] T. Mennecart, et al., Effect of alpha radiolysis on doped UO2 dissolution under reducing conditions, Radiochim. Acta 92 (9–11) (2004) 611–615.
[5] E. Ekeroth, O. Roth, M. Jonsson, The relative impact of radiolysis products in radiation induced oxidative dissolution of UO2, J. Nucl. Mater. 355 (1–3) (2006) 38–46.
[6] S. Nilsson, M. Jonsson, H2O2 and radiation induced dissolution of UO2 and Simfuel pellets, J. Nucl. Mater. 410 (1–3) (2011) 89–93.
[7] L. Bauhn, et al., The fate of hydroxyl radicals produced during H2O2 decomposition on a SIMFUEL surface in the presence of dissolved hydrogen, J. Nucl. Mater. 507 (2018) 38–43.
[8] C.M. Lousada, M. Trummer, M. Jonsson, Reactivity of H2O2 towards different UO2-based materials: the relative impact of radiolysis products revisited, J. Nucl. Mater. 434 (1–3) (2013) 434–439.
[9] J. Ziegler, Stopping of energetic light ions in elemental matter, J. Appl. Phys. 85 (3) (1999) 1249–1272.
[10] H. Bethe, Zur theorie des durchgangs schneller korpuskularstrahlen durch materie, Ann. Phys. 397 (3) (1930) 325–400.
[11] P. Sigmund, Stopping of Heavy ions: a Theoretical Approach Vol. 204 Springer Science & Business Media, 2004.
[12] Toftegaard, J., et al. Improvements in the stopping power library libdEdx and release of the web GUI dedx. au. dk. in Journal of Physics: Conference Series. 2014. IOP Publishing.
[13] M. Berger, et al., Report 37, J. Int. Commiss. Radiat. Units Meas. (2) (1984) NP–NP.
[14] J.F. Ziegler, Helium: Stopping Powers and Ranges in All Elemental Matter Vol. 4 Pergamon, 1977.
[15] Watt, D., Stopping cross sections, mass stopping powers and ranges in 30 elements for alpha particles (1keV to 100 MeV), in Internal Report of the University of St. Andrews. 1988.
[16] J.F. Ziegler, M.D. Ziegler, J.P. Biersack, SRIM–The stopping and range of ions in matter (2010), Nuclear Instrum. Methods Phys. Res. Sect. B: Beam Interact. Mater. Atoms 268 (11–12) (2010) 1818–1823.
[17] D. Emfietzoglou, et al., Subcellular S-factors for low-energy electrons: a comparison of Monte Carlo simulations and continuous-slowing-down calculations, Int. J. Radiat. Biol. 84 (12) (2008) 1034–1044.
[18] Cachoir, C., et al., Effect of alpha irradiation field on long-term corrosion rates of spent fuel. European commission framework program 1998-2002. Spent fuel stability under repository conditions. 2005.
[19] F. Hubert, R. Bimbot, H. Gauvin, Semi-empirical formulae for heavy ion stopping powers in solids in the intermediate energy range, Nuclear Instrum. Methods Phys. Res. Sect. B: Beam Interact. Mater. Atoms 36 (4) (1989) 357–363.
[20] J. Lindhard, M. Scharff, Energy dissipation by ions in the keV region, Phys. Rev. 124 (1) (1961) 128.
[21] D.C. Hansen, et al., Optimizing shield-hit for carbon ion treatment, Phys. Med. Biol. 57 (8) (2012) 2393.
[22] M. Tribet, S. Mougnaud, C. Jégou, Spent nuclear fuel/water interface behavior: alpha dose rate profile determination for model surfaces and microcracks by using Monte-Carlo methods, J. Nucl. Mater. 488 (2017) 245–251.
[23] Y. Kumazaki, et al., Determination of the mean excitation energy of water from proton beam ranges, Radiat. Meas. 42 (10) (2007) 1683–1691.
[24] F. Nielsen, M. Jonsson, Geometrical α-and β-dose distributions and production rates of radiolysis products in water in contact with spent nuclear fuel, J. Nucl. Mater. 359 (1–2) (2006) 1–7.
[25] M. Jansson, M. Jonsson, T. Eriksen, Basic Model of Geometrical Dose Distributions From Small UO2-particles, Swedish Nuclear Fuel and Waste Management Co. SKB U-96-44, 1994.
[26] F. Garisto, The energy spectrum of α-particles emitted from used CANDU^{TM} fuel, Ann. Nucl. Energy 16 (1) (1989) 33–38.
[27] L. Bauhn, et al., The interaction of molecular hydrogen with α-radiolytic oxidants on a (U, PU) O2 surface, J. Nucl. Mater. 505 (2018) 54–61.
[28] C. Jegou, et al., Effect of external gamma irradiation on dissolution of the spent UO2 fuel matrix, J. Nucl. Mater. 341 (1) (2005) 62–82.
[29] G. Sattonnay, et al., Alpha-radiolysis effects on UO2 alteration in water, J. Nucl. Mater. 288 (1) (2001) 11–19.
[30] D. Shoesmith, M. Kolar, F. King, A mixed-potential model to predict fuel (uranium dioxide) corrosion within a failed nuclear waste container, Corrosion 59 (9) (2003) 802–816.
[31] S. Sunder, Calculation of radiation dose rates in a water layer in contact with used Candu UO2 fuel, Nucl. Technol. 122 (2) (1998) 211–221.
[32] Spinks, J.W.T. and R.J. Woods, An introduction to radiation chemistry. 1990.
[33] V. Nitzki, H. Matzke, Stopping power of 1-9-MeV He+ + ions in UO 2,(U, Pu) O2, and ThO2, Phys. Rev. B 8 (5) (1973) 1894.
[34] M. Hosoe, et al., Stopping power measurement using thick alpha sources, Nuclear Instrum. Methods Phys. Res. 223 (2–3) (1984) 377–381.
[35] M. Matsumoto, T.J.A.T. Nishimura, C. Simulation, Mersenne twister: a 623-dimensionally equidistributed uniform pseudo-random number generator, Acm. T. Model. Comput. S. 8 (1) (1998) 3–30.
[36] M. Benedict, T. Pigford, H. Levi, *Nuclear Chemical Engineering*, 2nd Edition ed, McGraw-Hill, 1981.
[37] H. Christensen, Calculations simulating spent-fuel leaching experiments, Nucl. Technol 124 (2) (1998) 165–174.
[38] A. Poulesquen, C. Jégou, S. Peuget. Mater. Res. Soc. Symp. Proc., 932 (69.1) (2006).
[39] Lundgren, K., SKB Technical Report R-17-08, Radiation dose to water for an U-233 doped pellet compared to a long time decayed irradiated pellet. 2017.